

Cucumber-Like V_2O_5 /poly(3,4-ethylenedioxythiophene)& MnO_2 Nanowires with Enhanced Electrochemical Cyclability

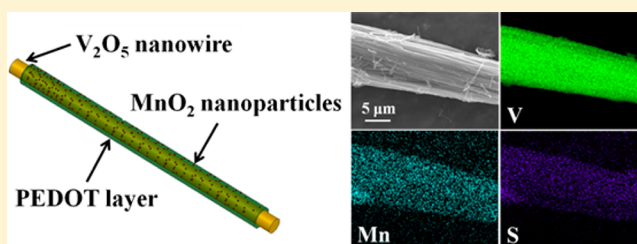
Liqiang Mai,* Fei Dong, Xu Xu, Yanzhu Luo, Qinyou An, Yunlong Zhao, Jie Pan, and Jingnan Yang

State Key Laboratory of Advanced Technology for Materials Synthesis and Processing, WUT-Harvard Joint Nano Key Laboratory, Wuhan University of Technology, Wuhan 430070, China

Supporting Information

ABSTRACT: Inspired by the cucumber-like structure, by combining the in situ chemical oxidative polymerization with facile soaking process, we designed the heterostructured nanomaterial with PEDOT as the shell and MnO_2 nanoparticles as the protuberance and synthesized the novel cucumber-like MnO_2 nanoparticles enriched vanadium pentoxide/poly(3,4-ethylenedioxythiophene) (PEDOT) coaxial nanowires. This heterostructured nanomaterial exhibits enhanced electrochemical cycling performance with the decreases of capacity fading during 200 cycles from 0.557 to 0.173% over V_2O_5 nanowires at the current density of 100 mA/g. This method is proven to be an effective technique for improving the electrochemical cycling performance and stability of nanowire electrodes especially at low rate for application in rechargeable lithium batteries.

KEYWORDS: Heterostructured nanomaterial, vanadium pentoxide/PEDOT, manganese oxide, layer-by-layer assembly, electrochemical property



In the past decades, rechargeable lithium (Li) batteries are widely considered to be among the most promising rechargeable batteries for the rapid development of mobile devices and electric vehicles.^{1–4}

Among the various candidates for cathode active materials in lithium batteries, vanadium oxides have attracted much attention due to their layered structure, high capacity (the theoretical capacity reaches 440 mAh/g when three lithium ions are intercalated) and low cost.^{5–9} For Li batteries, one-dimensional nanomaterial electrodes have drawn increasing attention because of their short Li ion diffusion pathway, favorably large electrode–electrolyte contact area and good strain accommodation.^{10–14} Although the nanostructured V_2O_5 has been studied as potential cathode material for almost 40 years, the poor electrical conductivity (4×10^{-4} S/cm) and low Li^+ ion diffusion rates still preclude its application.¹⁵ Hierarchical heterostructures such as hollow nanospheres, porous nanostructures, nanowire-on-nanowire structures, and so on have been increasingly reported in recent years because they can offer better electrochemical performance than single-structured materials.^{10,16–18} The cucumber-like structure with shell and rough surface is effective to protect the core structure and provides high active surface area. Inspired by the cucumber-like structure, we designed heterostructured nanomaterial by combining in situ chemical oxidative polymerization with facile soaking process to make use of the advantage of this cucumber-like structure.

Coating conductive polymers is an effective way to overcome the low electrical conductivity of V_2O_5 nanowires (NWs).^{19–21} Poly(3,4-ethylenedioxythiophene) (PEDOT) is one of the

most attractive conjugated conductive polymers. Nowadays, due to its high electrical conductivity (550 S/cm) and good electrochemical stability, PEDOT has drawn much attention from both fundamental and practical viewpoints. For example, PEDOT-coated Si NWs cause the capacity retention after 100 charge–discharge cycles to increase from 30 to 80% over bare Si NWs;²² the NWs- V_2O_5 /PEDOT composite film cathodes have high capacities, excellent rate capabilities, and cycling stabilities at various current rates.²³

Layer-by-layer (LBL) assembly is an attractive bottom-up approach to construct complex architecture and nanomaterials.²⁴ The advantages of the LBL assembly technique also include simplicity, universality, and controllable thickness at the nanoscale level, compared with the other available assembly approaches.²⁵ Nowadays the LBL assembly has been widely used to fabricate core–shell nanoparticles²⁶ and coaxial nanowires.²⁷

It was reported to form MnO_2 nanoparticles (NPs) on polymers by soaking in the potassium permanganate ($KMnO_4$).^{28–31} The nucleation of MnO_2 NPs over polymer chains can enhance conductivity and stability of the nanocomposite material by interlinking the polymer chains and providing high active surface area.³⁰ For example, MnO_2 nanoparticles-enriched PEDOT nanowires show very high specific capacitance (410 F/g) as the supercapacitor electrode materials, and high Li^+ storage capacity (300 mAh/g) as

Received: December 2, 2012

Revised: December 23, 2012

Published: January 11, 2013

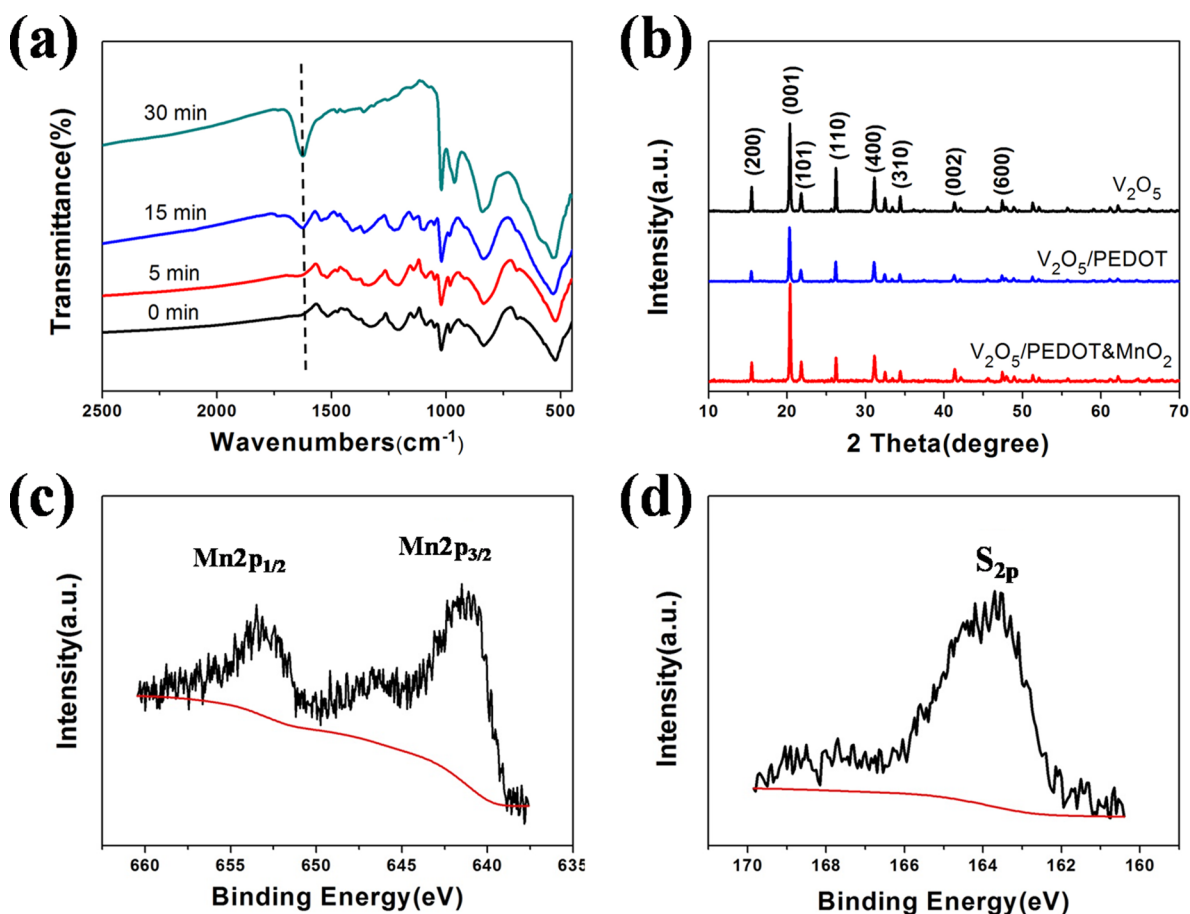


Figure 1. FTIR spectra of V_2O_5 /PEDOT&MnO₂ NWs for different soaking time (a), XRD patterns of V_2O_5 NWs, V_2O_5 /PEDOT NWs, and V_2O_5 /PEDOT&MnO₂ NWs (b), XPS spectra for V_2O_5 /PEDOT&MnO₂ NWs of Mn (c), and S (d).

cathode materials for Li ion battery, which boosts the energy storage capacity of PEDOT NWs 4 times;²⁹ PANI-intercalated manganese oxide shows high power performance as a kind of cathode material of lithium batteries.³¹ The advantages of this synthetic method are controllable thickness and no additional steps needed to prepare MnO₂ NPs before synthesizing the heterostructured material.²⁹

Herein, we report an LBL assembly method by combining the in situ chemical oxidative polymerization with facile soaking process to prepare cucumber-like MnO₂ NPs enriched V_2O_5 /PEDOT (V_2O_5 /PEDOT&MnO₂) NWs. This heterostructured nanomaterial exhibits enhanced electrochemical cycling performance with the decreases of capacity fading during 200 charge/discharge cycles from 0.557 to 0.173% over V_2O_5 NWs at the current density of 100 mA/g. This method is shown to be an effective technique for improving the electrochemical cycling performance and stability of nanowire electrodes especially at low rate for applications in rechargeable Li batteries.

The cucumber-like V_2O_5 /PEDOT&MnO₂ NWs were synthesized as follows. (1) Preparation of V_2O_5 NWs: the ultralong $V_3O_7 \cdot H_2O$ NWs were prepared by hydrothermal reaction following a previously reported procedure by Mai et al.³² Then the $V_3O_7 \cdot H_2O$ NWs were annealed under 500 °C for 5 h to obtain a yellow powder sample. (2) Preparation of V_2O_5 /PEDOT NWs: the PEDOT layer was prepared by in situ chemical oxidative polymerization. First, 0.1 g of as-prepared V_2O_5 NWs were dispersed in 40 mL of acetonitrile by agitation

and ultrasonic treatment and then transferred into a flask. Moreover, a certain number of EDOT monomers (mass ratio of V_2O_5 /EDOT is 1:0.3) were added and stirred with reflocculated V_2O_5 NWs for 1 h to ensure complete mixing. Additionally, a given amount of oxidizing agent (2 times of EDOT monomers in molar ratio) FeCl₃ was dispersed in 20 mL of acetonitrile, then added dropwise and kept under refluxing condition at 86 °C for 12 h. Then the products were washed repeatedly with ethanol and deionized water, and the dark green powder was dried at 60 °C for 12 h. (3) Preparation of V_2O_5 /PEDOT&MnO₂ NWs: MnO₂ NPs were loaded into the V_2O_5 /PEDOT NWs by soaking the as-prepared V_2O_5 /PEDOT NWs in 10 mM KMnO₄ solution. The mass of MnO₂ NPs was controlled by treating time. The treating time was chosen at 5, 15, and 30 min.

An X-ray diffraction (XRD) measurement was performed to investigate the crystallographic information using a D8 Advance X-ray diffractometer with nonmonochromated Cu K α X-ray source. Fourier transformed infrared (FTIR) transmittance spectra were recorded using the 60-SXB IR spectrometer. X-ray photoelectron spectroscopy (XPS) analysis was done on VG Multilab 2000. Field emission scanning electron microscopy (FESEM) images were collected with a Hitachi S-4800 at an acceleration voltage of 10 kV. Transmission electron microscopy (TEM), high-resolution transmission electron microscopy (HRTEM) images, and energy dispersive X-ray spectra (EDS) were recorded by using a JEM-2100F STEM/EDS microscope.

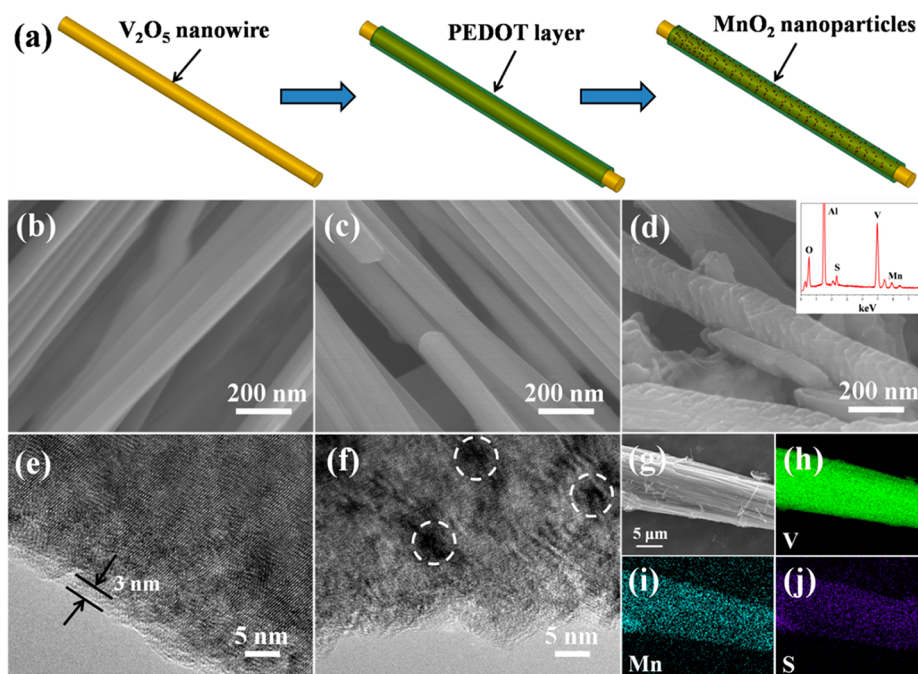
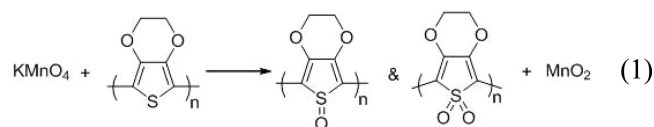


Figure 2. Schematic illustration of the synthesis of V_2O_5 /PEDOT&MnO₂ NWs (a), FESEM images of V_2O_5 NWs (b), V_2O_5 /PEDOT NWs (c), V_2O_5 /PEDOT&MnO₂ NWs (the inset is the EDS spectra) (d). TEM images of V_2O_5 /PEDOT NWs (e), V_2O_5 /PEDOT&MnO₂ NWs (f). FESEM image (g) and EDS mapping of V (h), Mn (i), and S (j) from V_2O_5 /PEDOT&MnO₂ NWs.

The electrochemical properties were tested with 2025 coin cells assembled in a glovebox filled with pure argon gas that use lithium pellet as the anode, 1 M solution of LiPF₆ in ethylene carbon (EC)/dimethyl carbonate (DMC) as the electrolyte, 70% V_2O_5 /PEDOT&MnO₂ nanowires active material, 20% acetylene black and 10% poly(tetrafluoroethylene) (PTFE) as the cathode electrodes. Galvanostatic charge/discharge measurement was performed in the potential range from 4.0 to 2.0 V versus Li/Li⁺ with a multichannel battery testing system (LAND CT2001A). Cyclic voltammetry (CV) and ac-impedance spectra were tested with an electrochemical workstation (CHI 760D).

FTIR spectra of the V_2O_5 /PEDOT&MnO₂ NWs with different soaking time (0, 5, 15, and 30 min) (Figure 1a) show the three vibration peaks of V_2O_5 around 1020, 835, and 525 cm⁻¹. Vibrations around 1540, 1470, and 1340 cm⁻¹ are assigned to the stretching modes of C=C and C-C in the thiophene ring; the peaks at 1200, 1140, and 1085 cm⁻¹ are attributed to C-O-C bond stretching mode, and the peaks at 980, 835, and 690 cm⁻¹ are attributed to the vibration transmittance of C-S bond in the thiophene ring. The 0 min curve (without soaking process) shows obvious peaks of PEDOT, illustrating the formation of PEDOT. Interestingly, a new peak around 1620 cm⁻¹ appears and becomes stronger with the increase of the soaking time, and meanwhile the peaks corresponding to PEDOT become weaker. The peak at 1620 cm⁻¹ is attributed to O-H stretching vibrations on a Mn atom,³³ which indicates possible oxidation of the PEDOT by KMnO₄ as eq 1 shows. In order to keep the electroactivity of PEDOT, the concentration of KMnO₄ and the soaking time should be controlled so that only a proper portion of the PEDOT can be oxidized. The soaking time of 15 min is considered as the optimal time parameter, because this product contains obvious vibration bonds of both PEDOT and Mn

atoms, so the following tests were based on the product by using 15 min soaking time.



To determine the phase structure of the products, XRD measurements were conducted (Figure 1b). The V_2O_5 NWs can be indexed to a pure orthorhombic structure phase (JCPDS No. 01-086-2248). No peaks from other phases have been detected, indicating that the products are of high purity. The characteristic peaks of V_2O_5 /PEDOT NWs have a consistent position with pure V_2O_5 , whereas the peak intensity decreases. The consistent peak position without shift shows that the formation of PEDOT on V_2O_5 NWs surface does not dramatically destroy the structure of V_2O_5 , and the intensity decrease can be explained by the formation of a PEDOT layer on the nanowire surface. XRD pattern of V_2O_5 /PEDOT&MnO₂ NWs only shows the pure orthorhombic V_2O_5 phase too, revealing that the MnO₂ NPs is amorphous. Compared with the V_2O_5 /PEDOT NWs curve, the intensity of (001) peak of V_2O_5 /PEDOT&MnO₂ NWs increased, which indicates that the preferred orientation of nanowires becomes relatively more obvious after the MnO₂ NPs were loaded.

The XPS spectra of V_2O_5 /PEDOT&MnO₂ NWs (Figure 1c,d) show the peaks of Mn2p_{3/2} and Mn2p_{1/2} (Figure 1c) centered at 641.5 and 653.5 eV, respectively, with a spin energy separation of 12 eV are in good agreement with reported data of Mn2p_{3/2} and Mn2p_{1/2} in MnO₂.^{30,34} Figure 1d shows that the peak of S_{2p} corresponds to PEDOT layer. A slight peak at 168 eV in XPS analysis alludes to the possible oxidation of thiophene sulfur into the sulfone S=O group,³⁵ which suggests possible oxidation of the thiophene sulfur into sulfoxide by KMnO₄ as eq 1 shows.

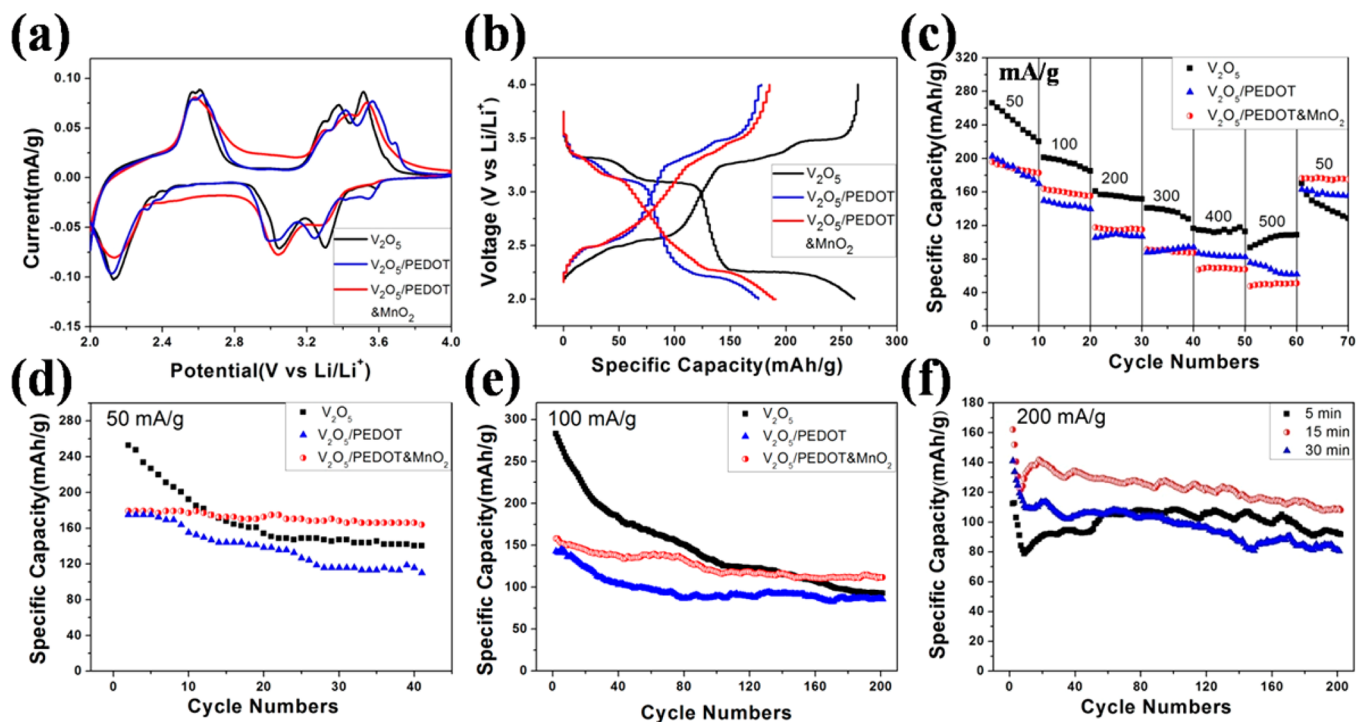


Figure 3. Electrochemical properties of V_2O_5 NWs, V_2O_5 /PEDOT NWs, and V_2O_5 /PEDOT&MnO₂ NWs. (a) CV curves at a sweep rate of 0.1 mV/s in the potential range from 4.0 to 2.0 V vs Li/Li⁺. (b) The initial charge–discharge curves at the current density of 50 mA/g. (c) The rate performance at various current densities from 50 to 500 mA/g. (d,e) The cycling performance at the current densities of 50 and 100 mA/g, respectively. (f) Discharge capacities of V_2O_5 /PEDOT&MnO₂ NWs with different soaking time at the current density of 200 mA/g.

The mechanism of MnO₂ formation is proposed as follows: we obtained the product with Mn/S molar ratio of 1.18 (from EDS analysis of Figure 2d inset), so 3.54 mol electrons should be provided to KMnO₄ to form 1.18 mol MnO₂. However, 1 mol PEDOT can only provide 0.3 mol delocalized electrons during the oxidation process,²⁹ thus the breakage of unsaturated bonds on PEDOT is unavoidable (eq 1), confirmed by the spectroscopic evidence from FTIR and XPS for the MnO₂ formation on the surface of PEDOT layer. The proposed mechanism coincides with the previously reported ones.^{29,36}

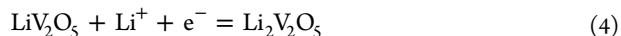
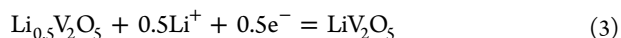
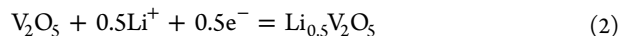
The cucumber-like structure of V_2O_5 /PEDOT&MnO₂ NWs by LBL assembly is shown in Figure 2. Figure 2a is the schematic illustration of the formation of a heterostructured nanowire. It is understandable that the core is V_2O_5 NWs, the layer is PEDOT prepared by in situ chemical oxidative polymerization, and the surface is loaded with MnO₂ NPs formed via the redox exchange of permanganate ions with the functional group on PEDOT by facile soaking. From the above results, the formation of heterostructured nanowires has been proved. This schematic illustration is in accordance with the FESEM and TEM images (Figure 2b,c,d).

The diameter of V_2O_5 NWs (Figure 2b) is around 150 nm, and the surface of the nanowires is very smooth. After PEDOT coated (Figure 2c), the diameter does not increase obviously. From the TEM image of V_2O_5 /PEDOT NWs (Figure 2e), the thickness of PEDOT layer is about 3–4 nm. Compared with V_2O_5 /PEDOT NWs (Figure 2c), V_2O_5 /PEDOT&MnO₂ NWs (Figure 2d) have rougher surfaces. Among the different soaking time (5, 15, and 30 min), the 15 min sample has the roughest surface (Supporting Information Figure S1), which provides the highest active surface area. The EDS spectrum of V_2O_5 /PEDOT&MnO₂ NWs (inset Figure 2d) reveals that molar ratio

of Mn to S is approximately 1.18:1, which suggests that a suitable number of MnO₂ NPs have been loaded into PEDOT layer. In the TEM image of the V_2O_5 /PEDOT&MnO₂ NWs (Figure 2f), some dark NPs are vaguely visible. The diameter of these NPs is around 5 nm and finely dispersed on the PEDOT layer. XRD studies show that the MnO₂ NPs are amorphous, but the TEM image shows that the NPs have weak crystalline, which may have formed due to bombardment caused by the TEM electron beams.²⁹

Energy dispersive X-ray spectrometry (EDS) mapping analysis (Figure 2h–j) of V_2O_5 /PEDOT&MnO₂ NWs (Figure 2g) unambiguously confirms the cucumber-like structure and the existence of Mn element. The mapping result is consistent with the EDS spectrum shown in the inset of Figure 2d.

The CV tests of V_2O_5 NWs, V_2O_5 /PEDOT NWs, and V_2O_5 /PEDOT&MnO₂ NWs for intercalation/deintercalation (Figure 3a) were carried out at a sweep rate of 0.1 mV/s in the voltage range of 4.0 to 2.0 V versus Li/Li⁺. As clearly shown in V_2O_5 NWs curves, during a cathodic scan three distinctive peaks are shown at 3.3, 3.1, and 2.1 V versus Li/Li⁺, which indicates a multistep lithium ion intercalation, and the corresponding phase is transformed from α - V_2O_5 to ϵ -Li_{0.5} V_2O_5 (3.3 V), δ -Li V_2O_5 (3.1 V), and γ -Li₂ V_2O_5 (2.1 V), consecutively.³⁷



The oxidation/reduction peaks of the three samples are around the same potential. The existence of MnO₂ (the oxidation/reduction peaks of MnO₂ are at 3.0/3.25 V) leads to a little bit shift of the peak of V_2O_5 /PEDOT&MnO₂ at 3.3 V.

The charge/discharge curves of V_2O_5 NWs, V_2O_5 /PEDOT NW, and V_2O_5 /PEDOT&MnO₂ NW cathodes at the current density of 50 mA/g are shown in Figure 3b. The initial discharge capacity of V_2O_5 NWs, V_2O_5 /PEDOT NWs, and V_2O_5 /PEDOT&MnO₂ NWs are 265, 178, and 185 mAh/g, respectively. Three discharge plateaus located around 3.3, 3.1, and 2.2 V can be well indentified as the transformation from α - V_2O_5 to ϵ -Li_{0.5} V_2O_5 (3.3 V), δ -Li V_2O_5 (3.1 V), and γ -Li V_2O_5 (2.2 V), respectively.

To study the rate during the charge/discharge process, the specific discharge capacities at different discharge/charge rates ranging from 50 to 500 mA/g were tested (Figure 3c). The V_2O_5 /PEDOT&MnO₂ NW cathode delivered the discharge capacities of 196, 164, 118, 91, 67, and 48 mAh/g at the current densities of 50, 100, 200, 300, 400, and 500 mA/g, respectively. After this rate measurement, the battery of V_2O_5 /PEDOT&MnO₂ NW cathode is able to provide the capacity of 176 mAh/g at 50 mA/g again, corresponding to the capacity retention of 90%. Compared with 64% of V_2O_5 NWs and 81% of V_2O_5 /PEDOT NWs, V_2O_5 /PEDOT&MnO₂ NWs show better rate stability.

At the current density of 50 mA/g (Figure 3d), the initial discharge capacities of V_2O_5 NWs, V_2O_5 /PEDOT NWs, and V_2O_5 /PEDOT&MnO₂ NWs are 253, 175, and 179 mAh/g, respectively. The discharge capacities decrease to 140, 116, and 166 mAh/g after 40 cycles, corresponding to the capacity fading per cycle of 1.462, 1.029, and 0.190%, respectively. It is obvious that the V_2O_5 /PEDOT&MnO₂ NWs exhibit the best cycling performance. The performance under the current density of 100 mA/g (Figure 3e) also displays as the similar phenomenon as that under the current density of 50 mA/g (the capacity fading per cycle of V_2O_5 /PEDOT&MnO₂ NWs after 200 charge/discharge cycles decreases from 0.557 to 0.173% over V_2O_5 NWs). After PEDOT coated, the initial specific capacity decreases about 70 mAh/g, owing to the introduction of low-capacity PEDOT component. At the same time, the capacity fading per cycle decreases because the PEDOT layer on the surface of V_2O_5 NWs overcomes the low electrical conductivity of V_2O_5 and also plays a role in protecting shell that prevents the collapse of V_2O_5 during the charge/discharge process. MnO₂ NPs enrichment increases the capacity retention of V_2O_5 /PEDOT NWs owing to the large specific surface area and high theoretical capacity of MnO₂. MnO₂ NPs can adsorb cations (Li⁺) on the electrode surface from electrolyte: $(MnO_2)_{\text{surface}} + Li^+ + e^- \leftrightarrow (MnOOLi)_{\text{surface}}$ and provide certain intercalation or deintercalation of Li⁺.^{38–40}

The cycling performance comparison of three V_2O_5 /PEDOT&MnO₂ NWs samples with different soaking time at the current density of 200 mA/g (Figure 3f) clearly shows that the sample with soaking for 15 min exhibits the highest capacity. The less the soaking time is, the less reaction time of V_2O_5 /PEDOT NWs has. The O–H stretching vibrations on a Mn atom at 1620 cm⁻¹ cannot be obviously observed from the 5 min curve in the FTIR spectra (Figure 1a), which illustrates that the PEDOT conjugated rings have not been broken and oxidized by KMnO₄. However, when the soaking time extends to 30 min, the capacity is lower than that of 15 min sample. The reason is that almost all of the unsaturated bonds on the PEDOT conjugated rings are broken and oxidized by KMnO₄, which destroys the conjugation of PEDOT, and further leads to the decrease of conductivity and electroactivity. This can be confirmed by FTIR spectra (Figure 1a) of 30 min sample.

In order to understand the enhanced electrochemical behavior, resistance components were analyzed by electrochemical impedance spectroscopic (EIS) studies. The Nyquist plots of V_2O_5 NWs, V_2O_5 /PEDOT NWs, and V_2O_5 /PEDOT&MnO₂ NW electrodes (Figure 4) indicate that all

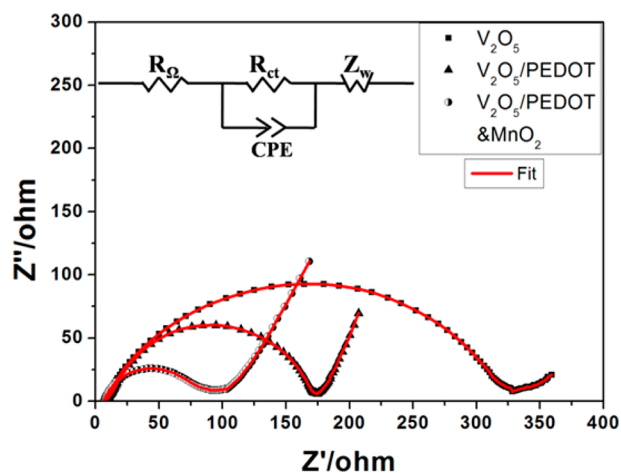


Figure 4. The ac-impedance spectra of V_2O_5 NWs, V_2O_5 /PEDOT NWs, and V_2O_5 /PEDOT&MnO₂ NWs.

of the electrodes show a semicircle at high-medium frequency and an inclined line at low frequency, which corresponds to charge transfer and diffusion respectively. A simple equivalent circuit model (inset of Figure 4) is built to analyze the impedance spectra of the three samples. In this circuit, R_Ω represents the Ohmic resistance of the electrode system, including the electrolyte and the cell components. R_{ct} represents the charge transfer resistance. CPE and Z_w are the double layer capacitance and the Warburg impedance, respectively. The transfer resistance of V_2O_5 NWs, V_2O_5 /PEDOT NWs, and V_2O_5 /PEDOT&MnO₂ NW electrodes are 309, 158 and 74 Ω , respectively. These suggest that the V_2O_5 /PEDOT&MnO₂ NWs have the lowest activation energy for the Li⁺ diffusion. The low R_{ct} for the V_2O_5 /PEDOT&MnO₂ NWs confirms the fast faradic reaction and high ionic conductivity.^{41–43}

In our case, the reasons why V_2O_5 /PEDOT&MnO₂ NW cathode displays enhanced electrochemical behavior can be explained as follows: (1) the PEDOT provides high electrical conductivity (550 $\Omega^{-1} \text{cm}^{-1}$) and good electrochemical stability; (2) the nucleation of MnO₂ NPs over PEDOT chains enhances the conductivity and stability of the nanocomposite material by interlinking the polymer chains and providing high active surface area; (3) amorphous MnO₂ on the surface enables the redox reaction reversible and the ion diffusion path shorter, and the PEDOT layer serves as a fast path for electron transport and increases the electrochemical utilization of amorphous MnO₂.

In summary, we successfully designed and synthesized the novel cucumber-like MnO₂ nanoparticles-enriched V_2O_5 /PEDOT coaxial nanowires by layer-by-layer assembly. On the basis of the spectroscopic evidence from FTIR and XPS, the formation of MnO₂ NPs is most likely triggered by the redox exchange of KMnO₄ with the sulfur sites on the PEDOT structures. The electrochemical performance investigation shows that the cucumber-like V_2O_5 /PEDOT&MnO₂ NWs exhibit enhanced electrochemical cycling properties as cathode

materials compared to that of V_2O_5 NWs due to more stable structure, higher active surface area, and shorter ion diffusion path. This method is proven to be an effective technique for improving the electrochemical cycling performance and stability of nanowire electrodes especially at low rate for applications in rechargeable lithium batteries.

■ ASSOCIATED CONTENT

■ Supporting Information

Additional information and figures. This material is available free of charge via the Internet at <http://pubs.acs.org>.

■ AUTHOR INFORMATION

Corresponding Author

*E-mail: mlq518@whut.edu.cn.

Notes

The authors declare no competing financial interest.

■ ACKNOWLEDGMENTS

This work was supported by the National Basic Research Program of China (2013CB934103, 2012CB933003), the National Natural Science Foundation of China (51272197 and 51072153), the International Science & Technology Cooperation Program of China (2013DFA50840), the Program for New Century Excellent Talents in University (NCET-10-0661), and the Fundamental Research Funds for the Central Universities (2012-II-001, 2012-YB-02). Thanks to Professor C. M. Lieber of Harvard University for strong support and stimulating discussion.

■ REFERENCES

- (1) Kang, B.; Ceder, G. *Nature* **2009**, *458*, 190.
- (2) Tarascon, J. M.; Armand, M. *Nature* **2001**, *414*, 359.
- (3) Liu, C.; Li, F.; Ma, L. P.; Cheng, H. M. *Adv. Mater.* **2010**, *22*, 28.
- (4) Ji, X.; Lee, K. T.; Nazar, L. F. *Nat. Mater.* **2009**, *8*, 500.
- (5) Mai, L. Q.; Xu, X.; Xu, L. *J. Mater. Res.* **2011**, *26*, 2175.
- (6) Gimenes, M. A.; Profeti, L. P. R.; Lassali, T. A. F. *Langmuir* **2001**, *6*, 1975.
- (7) Huguenin, F.; Ferreira, M.; Zucolotto, V.; Nart, F. C.; Torresi, R. M.; Oliveira, O. N. *Chem. Mater.* **2004**, *11*, 2293.
- (8) Mai, L. Q.; Lao, C. S.; Hu, B.; Zhou, J.; Qi, Y. Y.; Chen, W.; Gu, D.; Wang, Z. L. *J. Phys. Chem. B* **2006**, *110*, 18138.
- (9) Cui, C. J.; Wu, G. M.; Shen, J.; Zhou, B.; Zhang, Z. H.; Yang, H. Y.; She, S. F. *Electrochim. Acta* **2010**, *55*, 2536.
- (10) Mai, L. Q.; Xu, L.; Han, C. H.; Xu, X.; Luo, Y. Z.; Zhao, S. Y.; Zhao, Y. L. *Nano Lett.* **2010**, *10*, 4750.
- (11) Chan, C. K.; Peng, H. L.; Twisten, R. D.; Jarausch, K.; Zhang, X. F.; Cui, Y. *Nano Lett.* **2007**, *7*, 490.
- (12) Tian, B.; Xie, P.; Kempa, T. J.; Bell, D. C.; Lieber, C. M. *Nat. Nanotechnol.* **2009**, *4*, 824.
- (13) Dong, Y. J.; Tian, B. Z.; Kempa, T. J.; Lieber, C. M. *Nano Lett.* **2009**, *9*, 2183.
- (14) Xu, S.; Qin, Y.; Xu, C.; Wei, Y.; Yang, R.; Wang, Z. L. *Nat. Nanotechnol.* **2010**, *5*, 366.
- (15) Perera, S. D.; Patel, B.; Nijem, N.; Roodenko, K.; Seitz, O.; Ferraris, J. P.; Chabal, Y. J.; Balkus, K. J., Jr. *Adv. Energy Mater.* **2011**, *1*, 936.
- (16) Zhao, Y. L.; Xu, L.; Mai, L. Q.; Han, C. H.; An, Q. Y.; Xu, X.; Liu, X.; Zhang, Q. J. *Proc. Natl. Acad. Sci. U.S.A.* **2012**, *109*, 19569.
- (17) Mai, L. Q.; Yang, F.; Zhao, Y. L.; Xu, X.; Xu, L.; Luo, Y. Z. *Nat. Commun.* **2011**, *2*, 381.
- (18) Jiang, X. C.; Tian, B. Z.; Xiang, J.; Qian, F.; Zheng, G. F.; Wang, H. T.; Mai, L. Q.; Lieber, C. M. *Proc. Natl. Acad. Sci. U.S.A.* **2011**, *108*, 12212.
- (19) Gangopadhyay, R.; De, A. *Chem. Mater.* **2000**, *12*, 608.
- (20) Liu, R.; Lee, S. B. *J. Am. Chem. Soc.* **2008**, *130*, 2942.
- (21) Mai, L. Q.; Xu, X.; Han, C. H.; Luo, Y. Z.; Xu, L.; Wu, Y. A.; Zhao, Y. L. *Nano Lett.* **2011**, *11*, 4992.
- (22) Yao, Y.; Liu, N.; McDowell, M. T.; Pasta, M.; Cui, Y. *Energy Environ. Sci.* **2012**, *5*, 7927.
- (23) Song, H. M.; Yoo, D. Y.; Hong, S. K.; Kim, J. S.; Cho, W. I.; Mho, S. I. *Electroanalysis* **2011**, *23*, 2094.
- (24) Luo, W.; Hu, X. L.; Sun, Y. M.; Huang, Y. H. *J. Mater. Chem.* **2012**, *22*, 4910.
- (25) Srivastava, S.; Kotov, N. A. *Acc. Chem. Res.* **2008**, *41* (12), 1831.
- (26) Kim, J. S.; Rieter, W. J.; Taylor, K. M. L.; An, H.; Lin, W. L.; Lin, W. B. *J. Am. Chem. Soc.* **2007**, *129*, 8962.
- (27) Lathon, L. J.; Gudiksen, M. S.; Wang, C. L.; Lieber, C. M. *Nature* **2002**, *420*, 57.
- (28) Chen, S.; Zhu, J. W.; Wu, X. D.; Han, Q. F.; Wang, X. *ACS Nano* **2010**, *4* (5), 2822.
- (29) Liu, R.; Duay, J.; Lee, S. B. *ACS Nano* **2010**, *4* (7), 4299.
- (30) Sharma, R. K.; Rastogi, A. C.; Desu, S. B. *Electrochim. Acta* **2008**, *53*, 7690.
- (31) Wang, Y. G.; Wu, W.; Cheng, L.; He, P.; Wang, C. X.; Xia, Y. Y. *Adv. Mater.* **2008**, *20*, 2166.
- (32) Mai, L. Q.; Dong, Y. J.; Xu, L.; Han, C. H. *Nano Lett.* **2010**, *10*, 4273.
- (33) Han, J.; Li, L. Y.; Fang, P.; Guo, R. *J. Phys. Chem. C* **2012**, *116*, 15900.
- (34) Reddy, A. L. M.; Shaijumon, M. M.; Gowda, S. R.; Ajayan, P. M. *Nano Lett.* **2009**, *9*, 1002.
- (35) Gardella, J. A.; Ferguson, S. A.; Chin, R. L. *Appl. Spectrosc.* **1986**, *40*, 224.
- (36) Randriamahazaka, H.; Noël, V.; Chevrot, C. *J. Electroanal. Chem.* **1999**, *476*, 183.
- (37) Pan, A. Q.; Zhang, J. G.; Nie, Z. M.; Cao, G. Z.; Bruce, W. A.; Li, G. S.; Liang, S. Q.; Liu, J. *J. Mater. Chem.* **2010**, *20*, 9193.
- (38) Liu, J. P.; Jiang, J.; Cheng, C. W.; Li, H. X.; Zhang, J. X.; Gong, H.; Fan, H. J. *Adv. Mater.* **2011**, *23*, 2076.
- (39) Bao, L. H.; Zang, J. F.; Li, X. D. *Nano Lett.* **2011**, *11*, 1215–1220.
- (40) Yan, J.; Khoo, E.; Sumboja, A.; Lee, P. S. *ACS Nano* **2010**, *4*, 4247.
- (41) Hu, L. B.; Wu, H.; Gao, Y. F.; Cao, A. Y.; Li, H. B.; McDough, J.; Xie, X.; Zhou, M.; Cui, Y. *Adv. Energy Mater.* **2011**, *1*, 523.
- (42) Gnanaraj, J. S.; Thompson, R. W.; DiCarlo, J. F.; Abraham, K. M. *J. Electrochem. Soc.* **2007**, *154*, 185.
- (43) Choi, N. S.; Yao, Y.; Cui, Y.; Cho, J. *J. Mater. Chem.* **2011**, *21*, 9825.